Performance Analysis of RF Energy Harvesting NOMA Mobile Edge Computing in Multiple Devices IIoT Networks

Van-Truong Truong[1,2], Dac-Binh Ha[1,2], Tien-Vu Truong[3], and Anand Nayyar[4(✉)]

[1] Faculty of Electrical-Electronic Engineering, Duy Tan University, Da Nang 550000, Vietnam
truongvantruong@dtu.edu.vn, hadacbinh@duytan.edu.vn
[2] Institute of Research and Development, Duy Tan University, Da Nang 550000, Vietnam
[3] Faculty of Information Technology, Duy Tan University, Da Nang, Vietnam
truongtienvu@dtu.edu.vn
[4] Science and Technology Department, Duy Tan University, Da Nang, Vietnam
anandnayyar@duytan.edu.vn

Abstract. This paper considers the efficient offloading and computation design for radio frequency energy harvesting (RF EH) uplink non-orthogonal multiple access (NOMA) industrial Internet of Thing (IIoT) network. Specifically, the system contains multiple energy-constrained devices classified into two clusters and a MEC server deployed in a wireless access point (AP). We propose a four-phase communication protocol, namely EOCD, consisting of EH, task offloading, task computation, and information feedback transmission. Cluster head (CH) scheme is applied based on the channel information state to harvest RF energy from the AP in the first phase. In the second phase, CHs offload their workload to the AP using NOMA. The AP decodes the information signal and supports the computation of offload tasks in the third phase. Finally, AP feedbacks the result to each CH. Accordingly, we derive the closed-form expressions for the successful computation probability (SCP) of the considered system and CHs. We use Monte Carlo simulations to verify the results of the mathematical analysis. The numerical results demonstrate the effects of critical system parameters such as the time switching ratio, the transmit power, the number of devices in the cluster, and the task length of our proposed EOCD scheme compared to the conventional orthogonal multiple access (OMA) schemes.

Keywords: Mobile edge computing · Non-orthogonal multiple access · Uplink NOMA · Successful computation probability · Multiple devices

N.-S. Vo et al. (Eds.): INISCOM 2022, LNICST 444, pp. 62–76, 2022.
https://doi.org/10.1007/978-3-031-08878-0_5

1 Introduction

In recent years, Industry 4.0 has been effectively deployed in many industries such as automobile manufacturing, oil and gas exploitation, and warehouse management. Accordingly, the concept of IIoT was born with the leverage and reality of IoT in the context of industrial transformation and focused on guaranteeing real-time performance [1,2]. In IIoT paradigm, there are a massive number of mobile devices or machines connected and synchronized within the density network [3,4]. Moreover, many IIoT applications sponsored by local users can be very computation-intensive and latency-critical, e.g., smart factory, virtual reality, remote surgery, and autonomous car [5]. However, the finite battery life and the limited computation capacity of these devices pretend vital challenges. Mobile edge computing (MEC) is proposed, which enables edge users offload their task to MEC servers deployed at the edge network, can address the challenges mentioned above [6–8]. Moreover, the robust resource MEC servers can support energy or caching to ensure edge devices performance [9–11]. Therefore, the design of the MEC model needs a combination of the allocation of radio communication resources and devices computing resources, which is a complex problem and attracts much research attention [12]. Moreover, to further enhance the MEC offloading efficiency, a new multi-function MEC paradigm has been proposed, in which the MEC servers can employ different radio access networks (RANs) for wireless power charging and offloaded-task computing [13].

Since non-orthogonal multiple access (NOMA) outperforms compare to OMA in terms of spectral efficiency, supporting massive connectivity, and reduce latency [14], many researchers have proposed and evaluated system performance with NOMA MEC models [15–18]. For instance, Zhu *et al.* in [16] proposed a multi-user task offloading model in a NOMA MEC network. Specifically, a base station (BS) equipped with a MEC server assists N users with different task requests. The users are divided into L pairs, and each pair is allocated a time slot to offload the task using uplink NOMA. The authors proposed a matching-based user grouping algorithm and optimal power and time allocation that minimizes system energy consumption and delay. In [18], Xue *et al.* proposed the NOMA MEC multi-user multi-server system. The authors use the Lagrangian multiplier method to determine the optimal transmission power allocation to help the system achieve maximum offloading efficiency.

In addition, in an effort to develop a RAN system with self-sufficient devices, the radio frequency energy harvesting (RF EH) technique has been proposed [19]. This technique allows users to receive wireless power in the frequency bands from 3 KHz -3 GHz from BS or wireless access point (AP). Accordingly, edge users will be assured of energy for the computation and offloading processes, improving system performance. For instance, Vo *et al.* in [20] proposes a relay-based IoT network model using RF EH technique. The relays use power-splitting-based relaying for the EH process and forward information from a multi-antenna BS to the IoT sensor. The results show that this approach helps to improve system performance in terms of outage probability and throughput. More realistically, Vyas *et al.* in [21] proposed an RF EH prototype with an adaptive duty cycle

determination method for scavenging wireless power from TV signals at the distance of 6.5 km from the source.

However, the research on the design of multiple devices RF EH NOMA MEC networks has not been considered in the previous works. This motivated us to propose an RF EH and information transmission based devices selection and NOMA for multiple devices MEC IIoT systems. Accordingly, we analyze system performance by deriving the analytical expressions for successful computation probability (SCP) of system and each user. Our main contributions are as follows:

- We study the multiple devices RF EH NOMA MEC IIoT network over Rayleigh fading channel. Accordingly, we propose the four phase system protocol with CH approach, namely EOCD, to ensure the real-time performance.
- We derive the closed-form expression of successful computation probability (SCP) for the whole system and two CHs. Furthermore, we provided numerical results to investigate the impact of the network parameters, i.e., transmit power, time switching ratio, task length, bandwidth, to verify RF EH NOMA deployment's effectiveness in the MEC network.
- We compare the system performance between the EOCD and OMA scheme to clarify the outstanding performance of our proposed scheme.

The remainder of this paper is organized as follows. In Sect. 2, we introduce the system model and communication protocol for the multiple devices RF EH NOMA MEC IIoT systems. In Sect. 3, we perform the performance analysis in terms of SCP of whole system and each CHs. Section 4 presents simulation results and some discussion. Section 5 concludes the paper with future scope.

2 System Model

We consider an RF EH NOMA-aided computation offloading in a multiple IIoT devices (ID) MEC network as illustrated in Fig. 1. Specifically, a hybrid MEC server deployed in an access point (AP) to provide wireless power and offloading services for multiple IDs. The IDs are classified into two clusters, i.e., **A** and **B** to oversee different tasks in a smart factory. The cluster **A** has M IDs, denoted by $A_m, (m = 1, ..., M)$, which performs tasks of length L_{A_m}. Whereas cluster **B** has N IDs, denoted by $B_n, (n = 1, ..., N)$, performing tasks of length L_{B_n}.

Due to the characteristics of working in IIoT networks with a dynamic environment and mission-critical applications, IDs require an uninterrupted supply of energy and regular collection of ambient data, and timely delivery of control decisions [1,20]. Thus, the IDs in the network are equipped with hardware to harvest the RF energy of the AP to ensure continuous and seamless operation [9,22]. Since the computational capabilities of these IDs are limited, the users are assumed to offload their computationally intensive tasks to the hybrid MEC server. Furthermore, for reliability and redundancy, we assume each cluster monitors the same events and executes the same tasks, i.e., $L_{A_m} = L_1$ and $L_{B_n} = L_2$. All devices are assumed to be equipped with a single antenna and operate in the half-duplex mode [7,9].

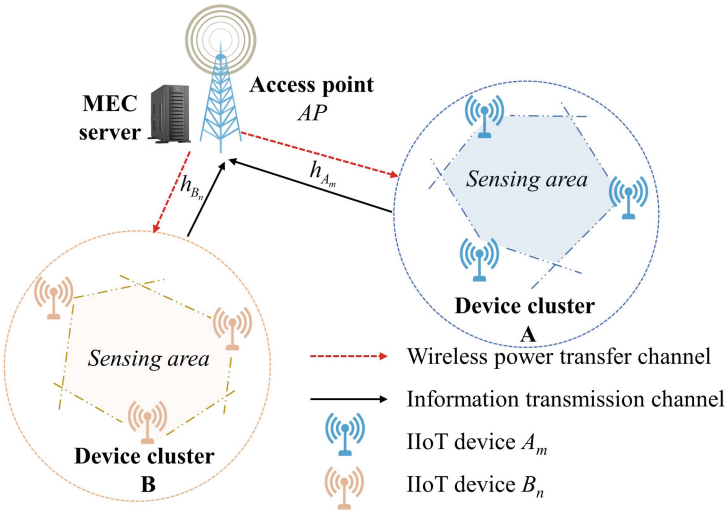

Fig. 1. Multiple devices RF EH NOMA MEC IIoT system model

2.1 Proposed Methodology

In this section, we propose a novel communication and offloading protocol, namely EOCD, for the proposed system. Following [8,9], we design a protocol that combines the offloading, communication, and computing processes in the NOMA MEC IIoT network to ensure energy and latency constraints.

Because AP and IDs are in the same MEC system with a short transmission distance, we assume AP has the full channel state information (CSI) of the system [8,9]. Before the communication takes place, AP sends a pilot signal to the IDs, and estimates the CSI of all links $\nu - AP, \nu \in \{A_n, B_m\}$. Based on the information collected, the AP selects the cluster head (CH) for each cluster so that the channel from the AP to each CH has the largest signal-to-noise ratio (SNR). The CHs representing the cluster send all their collected information to the AP. In the scope of this paper, we assume that the communication process between IDs and their CH has been resolved [23], and do not consider here.

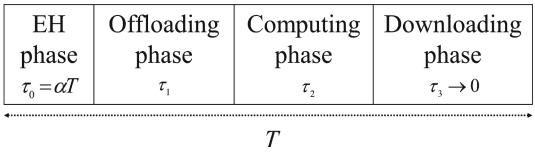

Fig. 2. Time flow chart of system protocol EOCD for proposed system

Let A^* and B^* be the CH of the cluster **A** and **B**, respectively. The formulas describe the indices of the CHs for communication as follows:

$$\begin{aligned} A^* &= \arg \max_{1 \le m \le M} \{g_{A_m}\}, \\ B^* &= \arg \max_{1 \le n \le N} \{g_{B_n}\}. \end{aligned} \tag{1}$$

The channel power gains of the CHs for communication as follows:

$$\begin{aligned} g_{A^*} &= \max_{1 \le m \le M} \{g_{A_m}\}, \\ g_{B^*} &= \max_{1 \le n \le N} \{g_{B_n}\}. \end{aligned} \tag{2}$$

Let $g_\nu, \nu \in \{A^*, B^*\}$ denotes the channel power gain of links $\nu - AP$. We assume that the links from AP to IDs are independent and modeled as Rayleigh fading channels. Thus g_ν are random variables that follow an exponential distribution. Accordingly, the probability density function (PDF) and cumulative distribution function (CDF) of g_ν are, respectively,

$$F_{g_\nu}(x) = \left(1 - e^{-\frac{x}{\lambda_\nu}}\right)^L = \sum_{l=0}^{L} \binom{L}{l} (-1)^l e^{-\frac{lx}{\lambda_\nu}}, \tag{3}$$

$$f_{g_\nu}(x) = \sum_{l=1}^{L} \binom{L}{l} \frac{(-1)^{l+1} l}{\lambda_\nu} e^{-\frac{lx}{\lambda_\nu}}, \tag{4}$$

where $L \in \{M, N\}$.

The system protocol EOCD, whose time flow chart is shown in Fig. 2, is divided into four phases in transmission time block T, as follows:

– *Phase 1 - EH phase:*
During this phase, A^* and B^* harvest RF energy from the AP for the period $\tau_0 = \alpha T$, where α denotes the time switching ratio, i.e., $0 < \alpha < 1$, and T stands for the threshold of latency. If the system is integrated with optimization algorithms, AP will calculate the EH time so that the system's performance is maximized. The energy obtained by the CHs in this process is:

$$E_\nu = \eta P_0 g_\nu \alpha T, \tag{5}$$

where $0 < \eta \le 1$ stands for the energy conversion efficiency of the energy receiver [9,24], P_0 denotes the transmit power of AP.

– *Phase 2 - Task offloading phase:*
This phase takes place in the period τ_1, in which CHs use all the energy collected in *Phase 1* to send their task to AP using uplink NOMA. Thus, the received superposition signal at AP is as follows:

$$y_{AP} = h_{A^*} \sqrt{P_{A^*}} x_A + h_{B^*} \sqrt{P_{B^*}} x_B + n_{AP}, \tag{6}$$

where h_ν denotes the channel coefficient of the link $\nu - AP$, x_ν stands for the offloading task of the CH ν, $\nu \in \{A^*, B^*\}$, $n_{AP} \sim \mathcal{CN}(0, \sigma^2)$ represents the AWGN at the AP. The transmit power of CHs is as follows

$$P_\nu = \frac{E_\nu}{(1-\alpha)T - \tau} = aP_0 g_\nu, \tag{7}$$

where $a \triangleq \frac{\eta\alpha T}{(1-\alpha)T-\tau}$, τ stands for the computing time at hybrid MEC server defined as follows:

$$\tau = \frac{\rho(L_1 + L_2)}{f}, \tag{8}$$

where ρ denotes the number of required CPU cycles for each input bit, and f is the CPU-cycle frequency of hybrid MEC server.

– *Phase 3 - Data computing phase:*
In this phase, the AP uses successive interference cancellation (SIC) to decode the superimposed signal to obtain useful signals from the CHs [15–17]. The AP decodes the higher-power level signal first and treat the lower-power level signal as noise. Continuing, the AP discards the decoded signal and receives the rest one. In this context, at AP exist two signal decoding scenarios described as follows:

- In the case the channel power gain of link $A^* - AP$ is better than channel power gain of link $B^* - AP$, i.e., $g_{A^*} > g_{B^*}$, AP applies SIC technique to decode x_A by treating the message x_B as noise. Then AP obtains x_B by subtracting x_A from received signal y_{AP}. Hence, the signal-to-interference-plus-noise ratio (SINR) and the SNR for the AP to decode $x_\nu, \nu \in \{A, B\}$ are written as:

$$\gamma_{11} = \frac{a\gamma_0 g_{A^*}^2}{a\gamma_0 g_{B^*}^2 + 1}, \tag{9}$$

$$\gamma_{12} = a\gamma_0 g_{B^*}^2, \tag{10}$$

  where $\gamma_0 = \frac{P_0}{\sigma^2}$.
- In the opposite case, i.e., $g_{A^*} < g_{B^*}$, the SINR and SNR for the AP to decode $x_\nu, \nu \in \{A, B\}$ are written as:

$$\gamma_{22} = \frac{a\gamma_0 g_{B^*}^2}{a\gamma_0 g_{A^*}^2 + 1}, \tag{11}$$

$$\gamma_{21} = a\gamma_0 g_{A^*}^2. \tag{12}$$

  The achievable channel capacity from CHs A^* and B^* to the AP is as:

$$\begin{cases} C_{11} = (1-\alpha)B\log(1+\gamma_{11}), \\ C_{12} = (1-\alpha)B\log(1+\gamma_{12}), & g_{A^*} > g_{B^*} \\ C_{21} = (1-\alpha)B\log(1+\gamma_{21}), \\ C_{22} = (1-\alpha)B\log(1+\gamma_{22}), & g_{A^*} < g_{B^*} \end{cases} \tag{13}$$

  where B denotes the channel bandwidth.

Then, these tasks are executed on the hybrid MEC server in duration τ_2.

– *Phase 4 - Downloading phase:*
Finally, in the last phase, CHs download the results from AP during τ_3. τ_3 is assumed very small compared to transmission time and thus is neglected [25].

3 Performance Analysis

Following [8,9,25], the successful computation probability (SCP), denoted by ϕ_s, of the RF EH NOMA MEC IIoT system is defined as the probability that the cluster's tasks are completed within the maximum delay time allows $T > 0$. Thus, we derive the formula of SCP as follow:

$$\phi_s = \Pr(\max(t_1, t_2) + \tau \leq T) \tag{14}$$

where t_1 and t_2 are the transmission latency of A^* and B^*, respectively and calculated as follows:

$$\begin{cases} t_1 = \frac{L_1}{C_{11}}, t_2 = \frac{L_2}{C_{12}}, & g_{A^*} > g_{B^*} \\ t_1 = \frac{L_1}{C_{21}}, t_2 = \frac{L_2}{C_{22}}, & g_{A^*} < g_{B^*} \end{cases} \tag{15}$$

We derive the SCP of two CHs and whole system as three Lemma.

Lemma 1. The closed-form expression of the SCP of CH A^*, denoted by $\phi_s^{A^*}$, for this considered system over quasi-static Rayleigh fading is as follow:

$$\phi_s^{A^*} = \begin{cases} \sum\limits_{MN} \left\{ \frac{n}{\lambda_{B_n}} \frac{\pi}{K} \sum\limits_{i=1}^{K} \exp\left(-\frac{m}{\lambda_{A_m}} \sqrt{\Psi_1} - \frac{n}{\lambda_{B_n}} \ln \frac{1}{x_i} \right) \sqrt{\frac{1-\phi_i}{1+\phi_i}} \right. \\ \left. + \frac{m\lambda_{B_n}}{m\lambda_{B_n} + n\lambda_{A_m}} \exp\left[-b_1 \left(\frac{m}{\lambda_{A_m}} + \frac{n}{\lambda_{B_n}} \right) \right] \right\}, \gamma_{th1} < 1 \\ \sum\limits_{MN} \left\{ \frac{n}{\lambda_{B_n}} \frac{\pi c_1}{2K} \sum\limits_{i=1}^{K} \exp\left(\frac{m}{\lambda_{A_m}} \sqrt{\Theta_1} - \frac{n}{\lambda_{B_n} y_i} \right) \sqrt{1-\phi_i^2} \right. \\ + \frac{n\lambda_{A_m}}{m\lambda_{B_n} + n\lambda_{A_m}} \exp\left[-c_1 \left(\frac{m}{\lambda_{A_m}} + \frac{n}{\lambda_{B_n}} \right) \right] \\ \left. + \frac{m\lambda_{B_n}}{m\lambda_{B_n} + n\lambda_{A_m}} \exp\left[-b_1 \left(\frac{m}{\lambda_{A_m}} + \frac{n}{\lambda_{B_n}} \right) \right] \right\}, \gamma_{th1} > 1 \end{cases} \tag{16}$$

where $\sum\limits_{MN} \triangleq - \sum\limits_{m=1}^{M} \sum\limits_{n=1}^{N} \binom{M}{m} \binom{N}{n} (-1)^{m+n+1}$, $\Psi_1 = \gamma_{th1} \left(\ln^2 \frac{1}{x_i} + \frac{1}{a\gamma_0} \right)$, $x_i = \frac{\phi_i + 1}{2}$, $\phi_i = cos(\frac{2i-1}{2K}\pi)$, $\gamma_{th1} = 2^{\frac{L_1}{(1-\alpha)B\Omega_1}} - 1$, $\Omega_1 = (1-\alpha)T - \tau_1$, $\tau_1 = \frac{\rho L_1}{f}$, $c_1 = \sqrt{\frac{\gamma_{th1}}{a\gamma_0(1-\gamma_{th1})}}$, $\Theta_1 = \gamma_{th1} y_i^2 + \frac{1}{a\gamma_0}$, $y_i = \frac{\phi_i + 1}{2} c_1$, $b_1 = \sqrt{\frac{\gamma_{th1}}{a\gamma_0}}$, K is the complexity-vs-accuracy trade-off coefficient.

Proof. See the Appendix A.

Lemma 2. The closed-form expression of the SCP of CH B_n^*, denoted by $\phi_s^{B^*}$, for this considered system over quasi-static Rayleigh fading is as follow

$$\phi_s^{B^*} = \begin{cases} \sum\limits_{MN} \left\{ \frac{m}{\lambda_{A_m}} \frac{\pi}{K} \sum\limits_{i=1}^{K} \exp\left(-\frac{n}{\lambda_{B_n}} \sqrt{\Psi_2} - \frac{m}{\lambda_{A_m}} \ln \frac{1}{x_i} \right) \sqrt{\frac{1-\phi_i}{1+\phi_i}} \right. \\ \left. + \frac{n\lambda_{A_m}}{m\lambda_{B_n} + n\lambda_{A_m}} \exp\left[-b_2 \left(\frac{m}{\lambda_{A_m}} + \frac{n}{\lambda_{B_n}} \right) \right] \right\}, \gamma_{th2} < 1 \\ \sum\limits_{MN} \left\{ \frac{m}{\lambda_{A_m}} \frac{\pi c_2}{2K} \sum\limits_{i=1}^{K} \exp\left(\frac{n}{\lambda_{B_n}} \sqrt{\Theta_2} - \frac{m}{\lambda_{A_m} y_i} \right) \sqrt{1-\phi_i^2} \right. \\ + \frac{m\lambda_{B_n}}{m\lambda_{B_n} + n\lambda_{A_m}} \exp\left[-c_2 \left(\frac{m}{\lambda_{A_m}} + \frac{n}{\lambda_{B_n}} \right) \right] \\ \left. + \frac{n\lambda_{A_m}}{m\lambda_{B_n} + n\lambda_{A_m}} \exp\left[-b_2 \left(\frac{m}{\lambda_{A_m}} + \frac{n}{\lambda_{B_n}} \right) \right] \right\}, \gamma_{th2} > 1 \end{cases} \tag{17}$$

where $\sum\limits_{MN} \triangleq - \sum\limits_{m=1}^{M} \sum\limits_{n=1}^{N} \binom{M}{m} \binom{N}{n} (-1)^{m+n+1}$, $\Psi_2 = \gamma_{th2} \left(\ln^2 \frac{1}{x_i} + \frac{1}{a\gamma_0} \right)$, $x_i = \frac{\phi_i + 1}{2}$, $\phi_i = cos(\frac{2i-1}{2K}\pi)$, $\gamma_{th2} = 2^{\frac{L_2}{(1-\alpha)B\Omega_2}} - 1$, $\Omega_2 = (1-\alpha)T - \tau_2$, $\tau_2 = \frac{\rho L_2}{f}$, $c_2 = \sqrt{\frac{\gamma_{th2}}{a\gamma_0(1-\gamma_{th2})}}$, $\Theta_2 = \gamma_{th2} y_i^2 + \frac{1}{a\gamma_0}$, $y_i = \frac{\phi_i + 1}{2} c_2$, $b_2 = \sqrt{\frac{\gamma_{th2}}{a\gamma_0}}$, K is the complexity-vs-accuracy trade-off coefficient.

Proof. The proof of Lemma 2 is similar to the proof of Lemma 1.

Lemma 3. The closed-form expression of the SCP of the considered system over quasi-static Rayleigh fading, denoted by ϕ_s, is as follow

$$\phi_s = \begin{cases} \sum\limits_{MN} \left\{ \frac{n}{\lambda_{B_n}} \frac{\pi}{K} \sum\limits_{i=1}^{K} \exp\left(-\frac{m}{\lambda_{A_m}} \sqrt{\Psi} - \frac{n}{\lambda_{B_n}} (b - \ln z_i) \right) \sqrt{\frac{1-\phi_i}{1+\phi_i}} \right. \\ \left. + \frac{m}{\lambda_{A_m}} \frac{\pi}{K} \sum\limits_{i=1}^{K} \exp\left(-\frac{n}{\lambda_{B_n}} \sqrt{\Psi} - \frac{m}{\lambda_{A_m}} (b - \ln z_i) \right) \sqrt{\frac{1-\phi_i}{1+\phi_i}} \right\}, \gamma_{th} > 1 \\ \sum\limits_{MN} \left\{ \exp\left[-c \left(\frac{m}{\lambda_{A_m}} + \frac{n}{\lambda_{B_n}} \right) \right] + \frac{n}{\lambda_{B_n}} \frac{\pi}{2K} (c-b) \sum\limits_{i=1}^{K} \exp\left(-\frac{m}{\lambda_{A_m}} \sqrt{\Theta} - \frac{n}{\lambda_{B_n}} t_i \right) \right. \\ \left. \times \sqrt{1-\phi_i^2} + \frac{m}{\lambda_{A_m}} \frac{\pi}{2K} (c-b) \sum\limits_{i=1}^{K} \exp\left(-\frac{n}{\lambda_{B_n}} \sqrt{\Theta} - \frac{m}{\lambda_{A_m}} t_i \right) \sqrt{1-\phi_i^2} \right\}, \gamma_{th} < 1 \end{cases} \tag{18}$$

where $\sum\limits_{MN} \triangleq - \sum\limits_{m=1}^{M} \sum\limits_{n=1}^{N} \binom{M}{m} \binom{N}{n} (-1)^{m+n+1}$, $\Psi = \gamma_{th} \left((b - \ln z_i)^2 + \frac{1}{a\gamma_0} \right)$, $\gamma_{th} = 2^{\frac{L}{(1-\alpha)B\Omega}} - 1$, $\Omega = (1-\alpha)T - \tau$, $\tau = \frac{\rho L}{f}$, $b = \sqrt{\frac{\gamma_{th}}{a\gamma_0}}$, $c = \sqrt{\frac{\gamma_{th}}{a\gamma_0(1-\gamma_{th})}}$, $\Theta = \gamma_{th} \left({t_i}^2 + \frac{1}{a\gamma_0} \right)$, $z_i = \frac{\phi_i + 1}{2}$, $\phi_i = cos(\frac{2i-1}{2K}\pi)$, $t_i = \frac{(\phi_i + 1)(c-b)}{2} + b$, K is the complexity-vs-accuracy trade-off coefficient.

Proof. The proof of Lemma 3 is similar to the proof of Lemma 1.

4 Numerical Results and Discussion

In this section, we present numerical results to confirm the accuracy of the theoretical results obtained for SCP. Unless otherwise specified, the system parameters are as follow: $P_0 = 10$ dB, $\alpha = 0.4$, $\eta = 0.6$, $\rho = 10$, $f = 1$ GHz, $B = 100$ MHz, $T = 10$ ms, $M = 3$, $N = 2$.

Figures 3a and 3b depict the SCP of each CH and whole system under the effect of time switching ratio (α) with different average transmit SNR (γ_0). We find that as γ_0 increases, the SCP for each CH and the whole system increases. In other words, increasing transmit power can help improve system performance. In addition, this figures show that α massively influences the SCP. If α is too small or too large, the system's SCP has a low value. Specifically, when α gradually increases from 0, the system's SCP tends to increase and reach maximum value. However, as α continues to grow too large, SCP drops. It can be explained that when α is low, CHs do not gather enough energy to function, resulting in low SCP. Nevertheless, when EH time is too large, i.e., α gets closer to 1, the offloading and computation processes no longer have enough time to complete, resulting in tasks that cannot be completed in time maximum allowable delay and SCP reduces.

We continue to compare the proposed system performance in two schemes, NOMA and OMA. In all three cases, the results show that the system operating under the NOMA scheme has significantly higher performance when operating under the OMA scheme.

Figures 4a and 4b depict the SCP of each CH and whole system under the effect of average transmit SNR (γ_0) with different time switching ratios (α). The obtained results once again confirm the observations in the above experiments. We observe that when γ_0 increases, that is, increases the transmit power of the AP, the system performance increases. However, when γ_0 grows too large, the system's SCP and CHs tend to saturate. Therefore, it is necessary to consider the design of the AP's transmits power appropriately while ensuring system performance in the proposed system. In all three investigating cases with different α, the SCP of the OMA scheme is much lower than the corresponding NOMA scheme. The curves are only asymptotic when γ_0 is very large. It proves the advantage of the NOMA-based system that we propose.

Figures 5a and 5b depict the impact of the number of IDs (M, N) on the SCP of the whole system and CHs. In Figs. 5a, we examine the system performance with five cases: the simplest case with one ID in each cluster, i.e., $(M, N) = (1, 1)$, (ii) increase the number of IDs in cluster **A**, i.e., $(M, N) = (3, 1)$, (iii) increase the number of IDs in cluster **B**, i.e., $(M, N) = (1, 3)$, (iv) increase the number of IDs in two cluster, i.e., $(M, N) = (3, 3)$, and (v) $(M, N) = (4, 4)$. The results show that increasing the number of IDs can significantly improve system performance. Specifically, the largest difference between the worst case (i) and the best case (v) is up to 60 %. It is consistent with the operating protocol of the system when the IDs are selected as the CH with the best transmission channel, thereby obtaining the most energy and participating in the most effective offloading process.

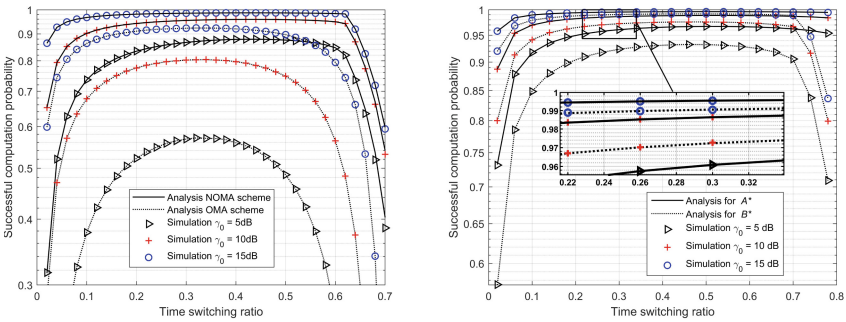

(a) System performance (b) CH performance

Fig. 3. The impact of time switching ratio on SCP with the different average transmit SNR.

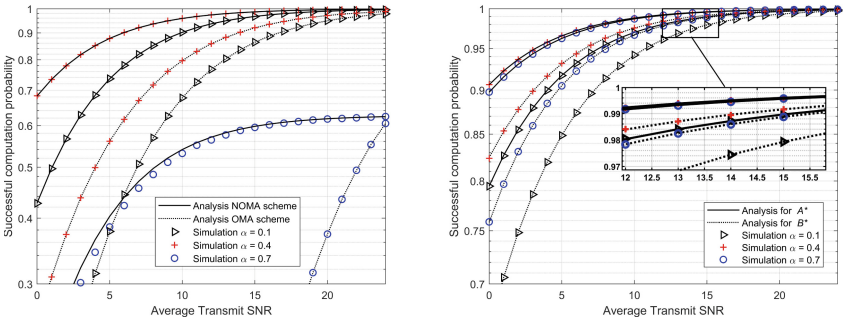

(a) System performance (b) CH performance

Fig. 4. The impact of average transmit SNR on SCP with the different time switching ratio.

However, when we compare the results in case (iv) and case (v), we notice that the performance improvement slows down as we continue to increase the number of IDs in each cluster. Furthermore, the effect of (M, N) on SCP is evident when γ_0 is low; this effect decreases as the transmit power increases. Another observation while we set the total number of users in the two clusters to be equal, i.e., case (ii) and case (iii), their system SCP is equal. It shows that the role of clusters in our proposed system is the same. The results obtained in Figs. 5b also give the same conclusion as above.

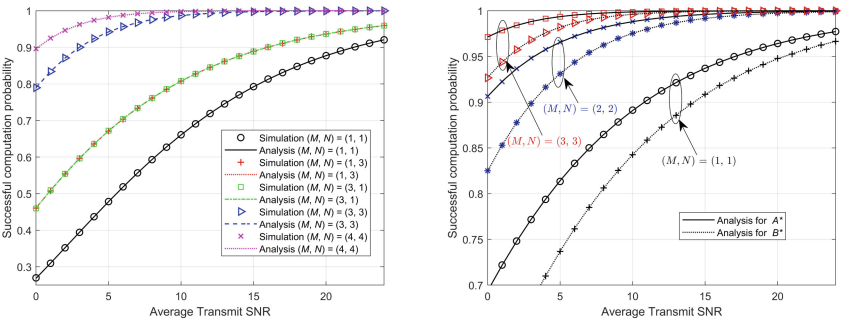

(a) System performance (b) CH performance

Fig. 5. The impact of average transmit SNR on SCP with the different number of IDs

Figure 6 depicts the SCP of the whole system under the effect of the length of task (L_1, L_2) with different bandwidth B. We observed that the more significant task length, the lower the performance of the system. The reason is that as L is more considerable, according to the formulas (8) and (15), the task offload time and computation time at the AP are more significant, resulting in AP not enough time to complete the task and respond to CHs. Another observation is that B has a significant hold on SCP. The larger the bandwidth, the better the system performance. It is entirely consistent with the formula (13); a high value of B means that the greater the achievable channel capacities from CHs to AP, the shorter the offloading time in enhancement system performance. Thus, when designing a MEC model, it is clear that the characteristics of the offloading tasks and channel bandwidth should be considered to achieve the required efficiency.

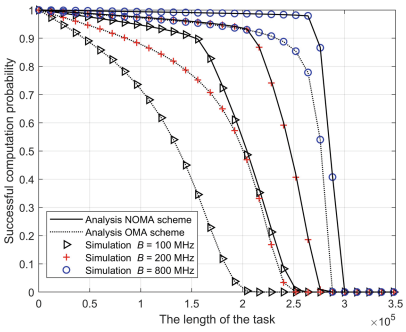

Fig. 6. The impact of the length of task on system SCP with the different bandwidth

The simulation results (Simulation) and analytical calculations (Analysis) are consistent in the above experiments, showing our research's correctness.

5 Conclusion

In this paper, we have proposed a novel network MEC IIoT scenario in which we used RF EH and NOMA for offloading tasks of multiple IDs to AP. Specifically, the IDs in each cluster select CHs to harvest the energy and offload their tasks over the Rayleigh fading channel. We derive the SCP of the whole system and two CHs and use them to evaluate system performance. The simulation results have shown that the EOCD scheme outperforms the existing OMA strategy, thus marking it an assuring candidate for carrying the functionality of the MEC IIoT scenarios. Specifically, system performance can be enhanced by implementing the following methods: (i) increase the transmit power of AP, (ii) increase the number of IDs in the clusters. Computational and theoretical results coincide, proving the accuracy of our study.

In future studies, we will investigate the system in the general case when the AP is equipped with many antennas. Furthermore, we will propose low complexity algorithms to find the optimal time switching ratio to help SCP reach its maximum value.

Acknowledgments. Van-Truong Truong was funded by Vingroup JSC and supported by the Master, PhD Scholarship Programme of Vingroup Innovation Foundation (VINIF), Institute of Big Data, code VINIF.2021.TS.049.

Appendix A: Proof of Lemma 1

Here, from equation (14) we derive the closed-form expression of $\phi_s^{A^*}$ as (A-0).

$$\begin{aligned}\phi_s^{A^*} &= \Pr\left(t_1 + \tau_1 \le (1-\alpha)T\right) \\ &= \underbrace{\Pr\left(g_1 > g_2, \gamma_{11} \ge \underbrace{2^{\frac{L_1}{(1-\alpha)B\Omega_1}} - 1}_{\gamma_{th1}}\right)}_{I_1} + \underbrace{\Pr\left(g_1 < g_2, \gamma_{21} \ge 2^{\frac{L_1}{(1-\alpha)B\Omega_1}} - 1\right)}_{I_2}.\end{aligned} \tag{A-0}$$

Using the properties of CDF and PDF, we implement I_1 as (A-1).

$$\begin{aligned}I_1 &= \Pr\left(g_1 > g_2, \frac{a\gamma_0 g_1^2}{a\gamma_0 g_2^2 + 1} > \gamma_{th1}\right) \\ &= \begin{cases} \underbrace{\int_0^\infty \left[1 - F_{g_1}\left(\sqrt{\gamma_{th1}\left(x^2 + \frac{1}{a\gamma_0}\right)}\right)\right] f_{g_2}(x)\,dx}_{I_{11}}, \gamma_{th1} < 1 \\ \underbrace{\int_0^{c_1} \left[1 - F_{g_1}\left(\sqrt{\gamma_{th1}\left(x^2 + \frac{1}{a\gamma_0}\right)}\right)\right] f_{g_2}(x)\,dx}_{I_{12}^a} + \underbrace{\int_{c_1}^\infty \left[1 - F_{g_1}(x)\right] f_{g_2}(x)\,dx}_{I_{12}^b}, \gamma_{th1} > 1 \end{cases}\end{aligned} \tag{A-1}$$

Using the Gaussian-Chebyshev quadrature method, we easily calculate I_{11} as (A-2).

$$I_{11} = -\sum_{m=1}^{M}\sum_{n=1}^{N}\binom{M}{m}\binom{N}{n}(-1)^{m+n+1}\frac{n}{\lambda_2}\frac{\pi}{K} \times \sum_{i=1}^{K}\exp\left(-\frac{m}{\lambda_1}\sqrt{\gamma_{th1}\left(\ln^2\frac{1}{x_i}+\frac{1}{a\gamma_0}\right)}-\frac{n}{\lambda_2}\ln\frac{1}{x_i}\right)\sqrt{\frac{1-\phi_i}{1+\phi_i}}, \tag{A-2}$$

where $x_i = \frac{\phi_i+1}{2}$, $\phi_i = cos(\frac{2i-1}{2K}\pi)$, K is the complexity-vs-accuracy trade-off coefficient. Using the same method, we calculate I_{12}^a and I_{12}^b as (A-3) and (A-4), respectively.

$$I_{12}^a = -\sum_{m=1}^{M}\sum_{n=1}^{N}\binom{M}{m}\binom{N}{n}(-1)^{m+n+1}\frac{n}{\lambda_2}\frac{\pi c_1}{2K} \times \sum_{i=1}^{K}\exp\left(\frac{m}{\lambda_1}\sqrt{\gamma_{th1}y_i^2+\frac{1}{a\gamma_0}}-\frac{n}{\lambda_2 y_i}\right)\sqrt{1-\phi_i^2}, \tag{A-3}$$

where $y_i = \frac{\phi_i+1}{2}c_1$, $\phi_i = cos(\frac{2i-1}{2K}\pi)$, K is the complexity-vs-accuracy trade-off coefficient.

$$I_{12}^b = -\sum_{m=1}^{M}\sum_{n=1}^{N}\binom{M}{m}\binom{N}{n}(-1)^{m+n+1}\frac{n\lambda_1}{m\lambda_2+n\lambda_1}\exp\left[-c_1\left(\frac{m}{\lambda_1}+\frac{n}{\lambda_2}\right)\right]. \tag{A-4}$$

Next, we focus to derive the closed-form expression of I_2 as (A-5).

$$I_2 = \Pr\left(\underbrace{\sqrt{\frac{\gamma_{th1}}{a\gamma_0}}}_{d_1} < g_1 < g_2\right) = \int_{d_1}^{\infty}\left[F_{g_1}(x) - F_{g_1}\left(\sqrt{\frac{\lambda_{th1}}{a\gamma_0}}\right)\right]f_{g_2}(x)\,dx = -\sum_{m=1}^{M}\sum_{n=1}^{N}\binom{M}{m}\binom{N}{n}(-1)^{m+n+1}\frac{m\lambda_2}{m\lambda_2+n\lambda_1}\exp\left[-d_1\left(\frac{m}{\lambda_1}+\frac{n}{\lambda_2}\right)\right]. \tag{A-5}$$

This concludes our proof.

References

1. Hou, X., Ren, Z., Yang, K., Chen, C., Zhang, H., Xiao, Y.: IIoT-MEC: a novel mobile edge computing framework for 5G-enabled IIoT. In: Proceedings of Wireless Communications and Network Conferences (WCNC), pp. 1–7. IEEE, Marrakesh, Morocco (2019)

2. Krishnamurthi, R., Kumar, A., Gopinathan, D., Nayyar, A., Qureshi, B.: An overview of IoT sensor data processing, fusion, and analysis techniques. Sensors **20**(21), 6076 (2020)
3. Chettri, L., Bera, R.: A comprehensive survey on Internet of Things (IoT) toward 5G wireless systems. IEEE Internet Things J. **7**(1), 16–32 (2019)
4. Elkashlan, M., Duong, T.Q., Chen, H.: Millimeter-wave communications for 5G–part 2: applications [Guest Editorial]. IEEE Commun. Mag. **53**(1): 166–167 (2015)
5. Mao, Y., You, C., Zhang, J., Huang, K., Letaief, K.B.: A survey on mobile edge computing: the communication perspective. IEEE Commun. Surv. Tut. **19**(4), 2322–2358 (2017)
6. Mach, P., Becvar, Z.: Mobile edge computing: a survey on architecture and computation offloading. IEEE Commun. Surv. Tut. **19**(3), 1628–1656 (2017)
7. Truong, V.T., Ha, D.B.: Secured scheme for RF energy harvesting mobile edge computing networks based on NOMA and access point selection. In: Proceedings of 7th NAFOSTED Conference on Information and Computer Science, pp. 7–12. IEEE, Ho Chi Minh City, Vietnam (2020). https://doi.org/10.1109/NICS51282.2020.9335833
8. Ha, D.-B., Truong, V.-T., Ha, D.-H.: A novel secure protocol for mobile edge computing network applied downlink NOMA. In: Vo, N.-S., Hoang, V.-P. (eds.) INISCOM 2020. LNICST, vol. 334, pp. 324–336. Springer, Cham (2020). https://doi.org/10.1007/978-3-030-63083-6_25
9. Truong, V.-T., Vo, M.-T., Ha, D.-B.: Performance analysis of mobile edge computing network applied uplink NOMA with RF energy harvesting. In: Vo, N.-S., Hoang, V.-P., Vien, Q.-T. (eds.) INISCOM 2021. LNICST, vol. 379, pp. 57–72. Springer, Cham (2021). https://doi.org/10.1007/978-3-030-77424-0_6
10. Yang, Z., Liu, Y., Chen, Y., Tyson, G.: Deep reinforcement learning in cache-aided MEC networks. In: ICC IEEE International Conference on Communication (ICC), pp. 1–6. IEEE, Shanghai, China (2019). https://doi.org/10.1109/ICC.2019.8761349
11. Tam, H.H.M., Tuan, H.D., Nasir, A.A., Duong, T.Q., Poor, H.V.: MIMO energy harvesting in full-duplex multi-user networks. IEEE Trans. Wirel. Commun. **16**(5), 3282–3297 (2017)
12. Sabella, D., Vaillant, A., Kuure, P., Rauschenbach, U., Giust, F.: Mobile-edge computing architecture: the role of MEC in the Internet of Things. IEEE Consum. Electron. Mag. **5**(4), 84–91 (2016)
13. Malik, R., Vu, M.: Energy-efficient joint wireless charging and computation offloading in MEC systems. IEEE J. Sel. Topics Signal Process. **15**, 1110–1125 (2021)
14. Wei, Z., Guo, J., Ng, D.W.K., Yuan, J.: Fairness comparison of uplink NOMA and OMA. In: Proceedings of IEEE 85th Vehicle Technology Conference, pp. 1–6. (IEEE) (VTC Spring) (2017)
15. Zhou, F., Wu, Y., Hu, R.Q., Qian, Y.: Computation efficiency in a wireless-powered Mobile Edge Computing network with NOMA. In: Proceedings IEEE International Conference on Communication (ICC), pp. 1–7. IEEE, Shanghai, China (2019). https://doi.org/10.1109/ICC.2019.8761172
16. Zhu, J., Wang, J., Huang, Y., Fang, F., Navaie, K., Ding, Z.: Resource allocation for hybrid NOMA MEC offloading. IEEE Trans. Wireless Commun. **19**(7), 4964–4977 (2020)
17. Fang, F., Xu, Y., Ding, Z., Shen, C., Peng, M., Karagiannidis, G.K.: Optimal resource allocation for delay minimization in NOMA-MEC networks. IEEE Trans. Commun. **68**(12), 7867–7881 (2020)

18. Xue, J., An, Y.: Joint task offloading and resource allocation for multi-task multi-server NOMA-MEC networks. IEEE Access **9**, 16152–16163 (2021)
19. Sidhu, R.K., Ubhi, J.S., Aggarwal, A.: A survey study of different RF energy sources for RF energy harvesting. In: Proceedings of International Conference on Automatic, Computer and Technological Management (ICACTM), pp. 530–533. IEEE, London, UK (2019). https://doi.org/10.1109/ICACTM.2019.8776726
20. So-In, C., Tran, H., Tran, D.D., Heng, S., Aimtongkham, P., Nguyen, A.N., et al.: On security and throughput for energy harvesting untrusted relays in IoT systems using NOMA. IEEE Access **7**, 149341–149354 (2019)
21. Vyas, R., Nishimoto, H., Tentzeris, M., Kawahara, Y., Asami, T.: A battery-less, energy harvesting device for long range scavenging of wireless power from terrestrial TV broadcasts. In Proceedings of IEEE/MTT-S International Microwave Symposium on Digest, pp. 1–3. IEEE, Montreal, QC, Canada (2012). https://doi.org/10.1109/MWSYM.2012.6259708
22. Rauniyar, A., Engelstad, P., Osterbo, O.N.: RF energy harvesting and information transmission based on NOMA for wireless powered IoT relay systems. Sensors **18**(10), 3254 (2018)
23. Al-Baz, A., El-Sayed, A.: A new algorithm for cluster head selection in LEACHs protocol for wireless sensor networks. Int. J. Commun. Syst. **31**(1), e3407 (2018)
24. Dac-Binh, H., Duc-Dung, T., Vu, T.H., Een-Kee, H.: Performance of amplify-and-forward relaying with wireless power transfer over dissimilar channels. Elektronika ir Elektrotechnika J. **21**(5), 90–95 (2015)
25. Ye, Y., Hu, R.Q., Lu, G., Shi, L.: Enhance latency-constrained computation in MEC networks using uplink NOMA. IEEE Trans. Commun. **68**(4), 2409–2425 (2020)